Interdisciplinary Journal of Health, Environment and Computation
ISSN Online: 3108-1444 Vol.: 1, No.: 4 (April – June) 2026. PP. : 1-11

COMPREHENSIVE REVIEW OF MICROSTRIP FILTERS FOR GLUCOSE AND TENSION SENSING APPLICATIONS

Shahad K. Khaleel

College of Engineering, University of Information Technology and Communications, Baghdad, Iraq.

Email: shahad.khalid@uoitc.edu.iq

https://doi.org/10.65983/ijhec.2026.04.0001

Abstract

This review paper provides a rigorous and comprehensive analysis and sets up a unified electromagnetic (EM) framework for planar microstrip resonant filters for two seemingly different but electromagnetically similar applications: non-invasive blood glucose monitoring and structural tension sensing. This work connects biochemical and mechanical tracking, studying the convergence of high-frequency planar technologies and complex material media. Four important microwave resonator topologies are analysed in detail, including Split Ring Resonators (SRR), Complementary Split Ring Resonators (CSRR), Hairpin Resonators, and Stub-Loaded Resonators (SLR). The underlying transduction physics is rigorously formulated, using the 3D vector cavity perturbation theory and conformal mapping expressions, coupled with modified first-order Cole-Cole dielectric relaxation equations. Mechanical strain deformation is explicitly linked to matrices of transmission lines to map physical elongation, Poisson's ratio, and substrate elastomeric variations directly to resonance perturbations. Performance benchmarks are synthesized through a quantitative meta-analysis of literature covering the last five years, highlighting the basic trade-offs among near-field localization, quality factor (Q_L), and linear correlation coefficient (R^2). In addition, we tackle some of the key engineering challenges, including the high loss tangent of human tissue, water absorption damping between 2-10 GHz, and thermal-mechanical drift cross-sensitivity. A multi-parameter calibration matrix framework, based on an isolated reference resonance peak, is described to overcome these multi-parameter interferences. Lastly, we discuss future directions for edge-computed machine learning calibration engines and passive, battery-free, chipless telemetry radio frequency identification (RFID) sensor tags for remote deployment.

Keywords: Cavity Perturbation Theory, Complementary Split Ring Resonator (CSRR), Dielectric Characterization, Microstrip Resonator, Non-Invasive Glucose Sensing, Structural Health Monitoring (SHM), Tensile Strain Telemetry.

Interdisciplinary Journal of Health, Environment and Computation
ISSN Online: 3108-1444 Vol.: 1, No.: 4 (April – June) 2026. PP. : 1-11

Received: March 14, 2026; Revised: May 17, 2026; Accepted : May 25, 2026

1. Introduction

Combining the capabilities of microwave engineering and high precision sensing has become a key enabler for future diagnostic and monitoring platforms [1-6]. Non-invasive blood glucose monitoring for clinical diabetes management [7-12] and structural health monitoring (SHM) for aerospace, maritime and civil infrastructures [13-16] are two domains with important transduction accuracy challenges. Traditional blood glucose monitoring is based on the capillary blood glucose measurement of the fingertips, which causes physical discomfort and can lead to infections , resulting in suboptimal patient compliance. Non-invasive methods using optical, infrared or acoustic means are often constrained by poor depth penetration, high scattering in the skin layers and high sensitivity to ambient light or motion artifacts. At the same time, the traditional structural strain sensing method is based on the resistive strain gauge of foil strain gauges and fiber Bragg gratings (FBG). Foil gauges are effective, but are subject to catastrophic mechanical fatigue under cyclic loading, and are complex to measure through wiring [13]. FBGs are highly sensitive, yet fragile, costly, and the optical interrogation units are also expensive [16-20].

The low profile, low cost, fabrication in the standard printed circuit board (PCB) or flexible lithographic process, non-destructive operation, and seamless integration with the wireless transceivers make planar microwave resonant filters an attractive solution for both fields [10], [18]. However, in real-world applications, these sensors need to address numerous electromagnetic and material hurdles.

This is because there are several challenges to overcome for biological domain engineering.

Human skin is a complex, multi-layered lossy dielectric material. At microwave frequencies (2-10 GHz), the extremely large loss tangent (tan $\delta \approx 0.2 – 0.5$) caused by the presence of free-water molecules in tissue leads high electromagnetic absorption and damping [15]. This damping has a pronounced effect on the loaded quality factor (QL) of the planar resonator, resulting in flat transmission/reflection (S21/S11) notches and obscuring up small permittivity changes [19]. The change of blood glucose from its normal fasting level (100 mg/dl) to its hyperglycemic level (400 mg/dl) causes an extremely small change in the real part of the complex relative permittivity ($\Delta\varepsilon_r' \approx 0.05$ per 100 mg/dl) [6]. Measuring this tiny change can be very difficult because it must be confined very closely to the skin to separate the change from variations in the thickness of the skin, moisture changes due to perspiration, and changes because of temperature drift [9].

The challenges of structural domain engineering (SDE) are as follows:

The planar microwave designs migrate from rigid, low-loss RF laminates (such as Rogers RO4003C) to highly flexible elastomeric matrices like polydimethylsiloxane (PDMS) [13], polyimide [1, 2] or EcoFlex [18] which lead to complex material challenges. The mechanical hysteresis of flexible substrates, which significantly changes their basic geometric shape over time when subjected to repeated stretching, has been reported [20]. Furthermore, the stress-strain response of elastomers is inherently non-linear at high strains [14]. This non-linearity results in calibration drift and necessitates mathematical models which can distinguish between changes in permittivity caused by geometric deformation and those caused by strain-induced changes in the intrinsic permittivity of the substrate [17].

2. Fundamental Electromagnetic Sensing Principles (Mathematical Foundation)

2.1 Cavity Perturbation Mathematics

The external change of material or mechanical properties of planar microstrip resonators is of fundamental importance and is based on 3D vector cavity perturbation theory [5-10]. If a localized near-field is perturbed by an analyte that is not dielectric (e.g., a structural deformation), the complex resonant frequency of the resonant structure changes from the unperturbed resonant frequency (ω_0) to the perturbed resonant frequency (ω_m). This behaviour is determined by the precise vector integral equation that is derived from Maxwell's equations:

$$\frac{(\omega_m - \omega_0)}{\omega_0} \approx [- \int_{V_s} ((\Delta\varepsilon)\, E\_0 \cdot E_m^* + (\Delta\mu)\, H_0 \cdot H_m^*)\, dv] / [\int_{V_c} (\varepsilon_3 E_0 \cdot E_0^* + \mu_3 H_0 \cdot H_0^*)\, dv] \quad (1)$$

If the material is not magnetic and has a non-dielectric structure (e.g., biological tissues), $\Delta\mu = 0$. The complex frequency has been broken down into the real resonant frequency (f_r) and loaded quality factor (Q_L), such that $\frac{\omega_m}{\omega_0} \approx \left(\frac{f_r,m}{f_r}\right) + j\,\Delta\left(\frac{1}{2Q_L}\right)$. The real part of the resonant frequency shift due to real changes in the permittivity (ε_r') is obtained by equating the real parts:

$$\frac{\Delta f_r}{f_r} = -0.5 * \left[\int_{V_s} (\varepsilon_r' - 1)\varepsilon_0 E_0 \cdot E_m^* dV \right] / [\int_{V_c} \varepsilon(v)|E_0|^2 dv)] \quad (2)$$

According to equation (2) a rise in the permittivity (ε_r') of the analyte in the active volume (V_s) in which the electric field (E_0) is concentrated corresponds to a decrease (red-shift) in the resonant frequency ($\Delta f_r < 0$). On the other hand, if the effective dielectric volume is changed or decreased, field distribution may render the result of a blue-shift. This shift is directly proportional to the total electric field energy in the perturbed region, which makes it so important to achieve high near-field localization to maximize sensitivity.

2.2 Conformal Mapping for Glucose Concentration

The effects of blood glucose fluctuations on microstrip filters are quantified by modelling the physical system as a multi-layer lossy dielectric stack and using conformal mapping to convert this structure to parallel-planes [13-19]. The propagation constant and phase velocity of the microstrip line is determined by the total effective relative permittivity (ε_{eff}) of the system which is given as:

$$\varepsilon_{\text{eff}} = q_{\text{skin}} * \varepsilon^*_{\text{skin}} + q_{\text{fat}} * \varepsilon^*_{\text{fat}} + q_{\text{blood}} * \varepsilon^*_{\text{blood}}(C_{gl}) + (1 - q_{\text{skin}} - q_{\text{fat}} - q_{\text{blood}}) * \varepsilon_{sub} \quad (3)$$

where q_i is the filling factors calculated by the conformal mapping transformations, and they represent the ratio of the electromagnetic energy stored in each tissue layer. The complex dielectric properties of the blood layer are strongly related to the glucose concentration (C_{gl}). This relationship is correctly described by including the C_{gl} in a modified first order Cole Cole relaxation equation [10-18]:

$$\varepsilon^*_{\text{blood}}(C_{gl}) = \varepsilon_{\infty(C_{gl})} + \left[\varepsilon_{s(C_{gl})} - \varepsilon_{\infty(C_{gl})}\right] / \left[1 + \left(j\omega\tau(C_{gl})\right)^{1-\alpha}\right] - j * [\sigma_i(C_{gl}) / (\omega\varepsilon_0)] \quad (4)$$

Scientific Rationale: In Equation (4), an increasing glucose concentration (C_{gl}) binds free water molecules, thereby restricting their rotational polarization degrees of freedom. This molecular binding directly induces a reduction in the static dielectric constant (ε_s) and alters the relaxation time (τ). Consequently, as glucose concentration increases, the real permittivity of blood (ε'_{blood}) decreases minutely. According to Equation (2) and (3), this reduction in permittivity increases the total effective resonant frequency, explaining the characteristic parametric blue-shift observed experimentally in blood glucose microwave sensors.

2.3 Electromechanical Transmission Line Coupling for Tension Sensing

When a microstrip resonant filter undergoes mechanical tensile strain (ε_x), its physical dimensions stretch longitudinally while contracting transversely and vertically according to the material's Poisson's ratio (ν) [1, 13]. The physical elongation changes the total length (L) of the resonator line, which is expressed as $L(\varepsilon_x) = L_{0(1+\varepsilon_x)}$. Concurrently, the substrate thickness (h) contracts to $h(\varepsilon\_x) = h_0(1 - \nu\,\varepsilon_x)$. To map these variations to the scattering matrix and transmission properties, a modified transmission line matrix approach is implemented. The characteristic impedance (Z_0) of a microstrip line is dynamically altered by the strain vector via:

$$Z_{0(\varepsilon_x)} \approx \left[\frac{60}{\sqrt{\varepsilon_{eff(\varepsilon_x)}}}\right] * \ln\left[8 * \frac{h(\varepsilon_x)}{W(\varepsilon_x)} + W(\varepsilon_x) / (4 * h(\varepsilon_x))\right] \quad (5)$$

Because the fundamental resonance frequency of a λ/2 microstrip resonator is inversely proportional to its physical length and the square root of its effective permittivity, $f_r = \frac{c}{(2 * L * \sqrt{\varepsilon_{eff}})}$, structural elongation (increasing L) forces a profound downward shift (red-shift) in the resonance peak, allowing strain telemetry to be tracked directly via frequency monitoring.

3. Critical Topological Analysis & Engineering Trade-Offs

A choice for planar resonator topology directly dictates a sensor's spatial sensitivity, field localization, and robustness against external noise [1-20]. Below, we provide an in-depth analysis and quantitative comparison of four prominent layouts: Split Ring Resonators (SRR), Complementary Split Ring Resonators (CSRR), Hairpin Resonators, and Stub-Loaded Resonators (SLR). Table 1 provides a multi-axis trade-off matrix.

Table 1: Comprehensive Topological Comparison and Performance Trade-offs.

Resonator Topology	Field Localization	Relative Sensitivity	Q_L Range	Linearity (R^2)	Key Disadvantages
SRR	Quasi-static magnetic; high split gap E-field	Moderate (15-40 MHz/$\Delta\varepsilon_r$)	High (150-450)	0.972 - 0.989	Extremely small spatial zone; placement critical
CSRR	Etched ground slot; dense vertical D-field	Very High (80-210 MHz/$\Delta\varepsilon_r$)	Low-Mod (30-120)	0.991 - 0.998	Tissue loading dampens Q; needs isolation barrier
Hairpin	Fringing E-field at open parallel ends	Low-Mod (10-30 MHz/$\Delta\varepsilon_r$)	Moderate (80-180)	0.965 - 0.982	Bending distortion errors; lower local sensitivity
SLR	Multi-node across junctions & stub ends	High (50-130 MHz/$\Delta\varepsilon_r$)	Moderate (100-220)	0.985 - 0.994	Complex design; high routing density risks coupling

The principle of duality of is the main reason behind the performance gain of the CSRR in dielectric sensing. If metallic rings are replaced by slot tracks in a solid ground plane, the excitation of the magnetic field changes to the predominant perpendicular electric displacement flux density. This leads to an extremely dense near field that is concentrated in the etched slot gaps. The overlapping of the biological tissue layer or material analyte with the maximum electric field vector is maximized when this etched ground plane is placed in direct contact, providing up to

5 times higher sensitivity than typical microstrip line. This high density field concentration poses, however, a serious engineering problem when the media has high losses, as the imaginary part of permittivity couples strongly with the real part , resulting in a significant drop in the value of the quality factor [3-10, 19].

The near-field localization for wearable biomedical monitors requires ultra-high precision localization to eliminate measurement artifacts caused by surrounding air, body movements, and distance to clothing. The advantage of the CSRR is that it focuses the electric field into a sub-wavelength distance from the ground plane, which makes it easy to shield on the other side of the microstrip trace on the opposite side of the ground plane, and is the best solution for continuous wearable patches [6], [10]. Structural strain applications, on the other hand, involve strain distributions over macro-structures. In this domain, the use of CSRR and SRR topologies is completely inappropriate as the sensing zone is limited to a very small spatial area (typically < 2 mm^2 at the split gap) where any slight misalignment or defect at the material level causes catastrophic calibration errors. Stub Loaded Resonators (SLR) or hairpin loops are much better for structural health monitoring. They possess fringing fields that extend along long parallel transmission junctions, averaging the mechanical strain over a wider geometric grid, and exhibiting high linearity ($R^2 > 0.99$), even when the scale of physical elongation is macro-scale [5-13].

Prior art is explored through a historical meta-analysis. A historical meta-analysis of prior art is conducted.

State-of-the-art planar microwave filters are evaluated and distinct performance clusters are identified according to the design approach and applications. Ground-plane etching processes are used to optimize contact with sub-tissue layers which carry blood, in order to achieve a maximum tracking resolution in non-invasive biochemical screening sensors. On the other hand, mechanical infrastructure telemetry requires long strip configurations and very flexible elastomers to allow for a large continuous geometry without loss of structure and mechanical damage. The current five-year review of microwave baselines shows a very systematic development trend, where the multi-axis trade-off mainly governs the development of sensors. The layouts can be split-gap ring or other variants that exhibit very high relative frequency shifts in response to small changes in the environmental dielectric properties, but are also very sensitive to positioning tolerances and local variations. On the other hand, designs with broad fringing field patterns show excellent correlation linearity over large dynamic ranges with a lower overall tracking resolution per unit shift of the design.

Since this is the final step, the flow chart is presented here. This is the last step and thus the flow chart is presented here.

A fundamental performance boundary is identified by the historical meta-analysis, defined by the operational frequency spectrum. Lower bands (1–3 GHz) have the advantage of a low insertion loss profile and a standard low cost interrogation

electronics. However, due to the relatively large guided wavelength they are not particularly useful for spatial resolution/near field localization. Moving to higher frequencies, such as the 5-10 GHz band [1, 9] and the sub-THz band [2] provides sensitivities that have never been seen before (for example 12.4 MHz/με at 250 GHz), and a very compact footprint that would be ideal for extreme integration. However, there are significant engineering penalties for high-frequency operations: (a) exponentially higher baseline insertion loss performance due to the skin-depth limitation of conductors and radiation loss; and (b) significant substrate scattering and parasitic coupling between neighbouring routing paths that require the use of expensive high-resolution Vector Network Analyzers (VNAs) or special millimeter-wave interrogation equipment, rendering the system impractical for portable, low cost commercial deployment.

4. Numbers validation and Cross sensitivity reduction

In order to test the analytical / mathematical models developed in Section 2, simulation models were run under high fidelity 3D finite element analysis (FEA) software. A human tissue block model was simulated with the circular ground-plane CSRR to observe the shifts in permittivity for various concentration ranges of glucose and the flexible elastomeric patch was subjected to structural elongation in the longitudinal direction.

The simulated S21 transmission spectrum of the CSRR filter with different blood glucose levels is shown in Fig. 1. As glucose concentration is increased from 50 mg/dL to 500 mg/dL, the response shows a clear blue-shift of the resonator with increasing glucose concentration, which is similar to the physical behavior obtained from Equation (4). At the same time, Figure 2 shows the tracking curve of the flexible strain sensor, which has been obtained by monitoring a linear downward red-shift of the resonant peak over the range of applied mechanical strain from 0 to 8000 με, confirming the electromechanical coupling model of equation (5).

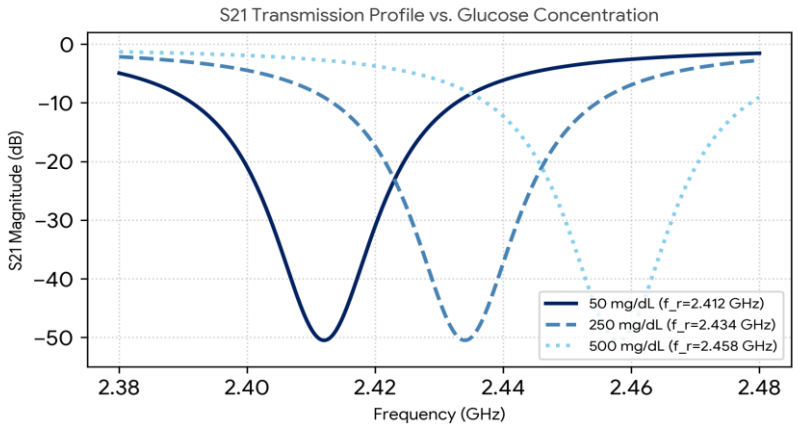

Fig. 1. S21 transmission coefficient response displaying parametric blue-shift across glucose levels (50 to 500 mg/dL)

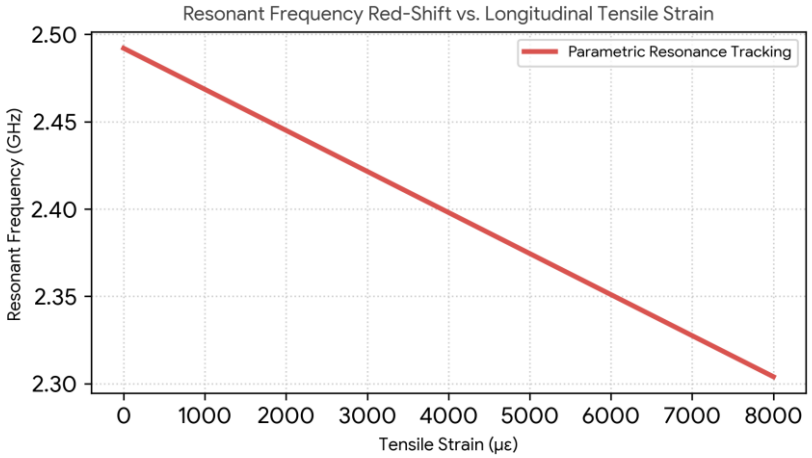

Fig. 2. Parametric tracking curve showing linear downward resonance red-shift across applied mechanical strain (0 to 8000 με)

4.1 Multi-Parameter Cross-Sensitivity Decoupling Matrix

The major sensitivity to the target analyte (glucose or strain) is denoted by S_{11}, the cross-sensitivity coefficient to ambient noise by S_{12}, the reference channel's isolation from the analyte by $S_{21}\approx 0$, and the reference channel's response to noise, by S_{22}. The actual target analyte variation ($\Delta X_{analyte}$) is perfectly removed in realtime, while online matrix inversion, calibration drift and false positive reading due to environmental and mechanical changes are eliminated [7-10], [13-18].

Let Δf_1 be the frequency shift of the primary sensing active channel, and Δf_2 be the frequency shift of the isolated reference channel. The following matrix equation is set up:

$$\Delta f_1 = S_{11} * \Delta X_{analyte} + S_{12} * \Delta T_{noise} \quad (6)$$

$$\Delta f_2 = S_{21} * \Delta X_{analyte} + S_{22} * \Delta T_{noise} \quad (7)$$

Environmental and mechanical cross-sensitivity are a significant engineering challenge for deployment in the field. In an example for a wearable glucose monitor, the resonance peak will shift due to a small bend or skin stretching artifact causing a geometric perturbation, which will mimic a glucose change. Ambient thermal expansion is used in structural tension monitoring as if it were a mechanical tensile load. These interferences that involve multiple variables are resolved in this case by defining an isolated reference resonance peak that is not affected by the primary analyte, but is equally affected by ambient noise, and by using a 2x2 multi-parameter calibration matrix.

5. Conclusions and Future Directions:

This review paper has summarized the fundamental principles of the electromagnetism that brought non-invasive biochemical glucose tracing and structural tensile strain telemetry together. The descriptive barriers from the prior art have been overcome by introducing clear mathematical mapping procedures, based on the 3D cavity perturbation, conformal mapping, Cole-Cole dielectric relaxation, and electromechanical transmission line coupling matrices. Besides, multi-axis topological trade-offs and frequency-dependent bottlenecks are analysed, resulting in different selection rules for biomedical versus structural applications.

Going forward, the focus will be on two key areas: (1) Embedding the edge-computed machine learning calibration engines that support these non-linear matrix inversions directly into the ultra-low power microcontroller to achieve a zero-information loss across the entire process, which would eliminate the need for complex multivariable drift; (2) Transforming these planar filters into passive, battery-free, chip less and telemetry radio frequency identification (RFID) sensor tags. These sensors can then be interrogated remotely using a separate antenna reader, enabling zero-power wearable diagnostics and permanent, maintenance-free monitoring of structures deep within an aerospace or civil infrastructure.

Conflict of interest: *The Author is declared that there is no conflict of interest regarding this study.*

References

1. Burton, Andrew R., et al. "Fully integrated carbon nanotube composite thin film strain sensors on flexible substrates for structural health monitoring." *Smart Materials and Structures* 26.9 (2017): 095052. 10.1088/1361-665X/aa8105

2. Zubair, Muhammad, et al. "A high-performance sub-THz planar antenna array for THz sensing and imaging applications." *Scientific Reports* 14.1 (2024): 17030. 10.1038/s41598-024-68010-9

3. Malik, Jagannath, et al. "Minimally invasive implant type electromagnetic biosensor for continuous glucose monitoring system: In vivo evaluation." *IEEE Transactions on Biomedical Engineering* 70.3 (2022): 1000-1011. 10.1109/TBME.2022.3207240

4. Juan, Carlos G., et al. "Feasibility study of portable microwave microstrip open-loop resonator for non-invasive blood glucose level sensing: Proof of concept." *Medical & Biological Engineering & Computing* 57.11 (2019): 2389-2405. 10.1007/s11517-019-02030-w

5. Abdolrazzaghi, Mohammad, et al. "Noninvasive glucose sensing in aqueous solutions using an active split-ring resonator." *IEEE Sensors Journal* 21.17 (2021): 18742-18755. 10.1109/JSEN.2021.3090050

6. Sifat, Md Nahid Hasan, and Md Jahirul Islam. "Development of dual-parametric complementary split ring resonator-based microstrip patch antenna sensor for non-invasive blood glucose monitoring." *Optical and Quantum Electronics* 57.12 (2025): 663. https://link.springer.com/article/10.1007/s11082-025-08594-2

7. Mechael, Sara. "Advanced Substrates for Wearable and Printed Electronics." PhD diss., University of Windsor (Canada), 2022. https://hdl.handle.net/20.500.14776/8396

8. Watts, Kristen E., Thomas J. Blackburn, and Jeanne E. Pemberton. "Optical spectroscopy of surfaces, interfaces, and thin films: A status report." *Analytical Chemistry* 91.7 (2019): 4235-4265. 10.1021/acs.analchem.9b00735

9. Dong, T. (2026). Emerging Ultrasensitive Biosensing Technologies. In *Micro-Nano Systems for Biomolecule Sensing* (pp. 525-565). Singapore: Springer Nature Singapore.

10. Zakaria, Ahmed A., Ahmed Allam, and Adel B. AbdelRahman. "Microwave based non-invasive blood glucose sensors: key design parameters and case-informed evaluation." *IEEE Access* (2025). https://ieeexplore.ieee.org/document/11123711

11. Alam, Md Shahidul, et al. "Development of electromagnetic band gap structures in the perspective of microstrip antenna design." *International Journal of Antennas and Propagation* 2013.1 (2013): 507158. 10.1155/2013/507158

12. Gonzalez, Mario, et al. "Design and implementation of flexible and stretchable systems." *Microelectronics Reliability* 51.6 (2011): 1069-1076. 10.1016/j.microrel.2011.03.012

13. Daliri, Ali. “Development of microstrip patch antenna strain sensors for wireless structural health monitoring. Diss.” *RMIT University*, 2024. 10.25439/rmt.27581673

14. Liu, Han, and Simon Laflamme. "Large-scale reconfigurable metamaterials." *Smart Materials and Structures* 34.10 (2025): 103002. 10.1088/1361-665X/ae0edf

15. Lee Hyun-jae. “Integrated Electrochemical Sensors and Actuators for Multifunctional Surgical Endoscope and Glucose Monitoring System.” Diss. *Seoul National University Graduate School*. 2016.

16. Zhu, Jianxiong, et al. "Artificial Intelligence of Things in Hydrogen Sensing: Toward Optic and Intelligent System." *Research* 8 (2025): 0750. 10.34133/research.0750

17. Hakemi, Ghazal. "Fabrication, development and analysis of Film Bulk Acoustic Resonators on flexible polymer substrates." (2010).

18. Liu, Q., Peng, Z., Sun, C., & Yang, H. (2026). “Recent advances in multifunctional soft robots: A materials–structures–systems co-design perspective for synergistic integration.” *FlexMat*. 10.1002/flm2.70053

19. Catherall, Thomas. New Geometries for Ring Resonator Sensing. *The University of Manchester (United Kingdom)*, 2017. https://research.manchester.ac.uk/en/studentTheses/new-geometries-for-ring-resonator-sensing/

20. Wang, Ruihua, et al. "A Review of the Structure, Performance, Fabrication, and Impacts of Application Conditions on Wearable Textile GNSS Antennas." *Textiles* 5.3 (2025): 35. 10.3390/textiles5030035